nanomaterials

MDPI

Review

Avalanche Multiplication in Two-Dimensional Layered Materials: Principles and Applications

Zhangxinyu Zhou [1,2,†], Mengyang Kang [1,3,†], Yueyue Fang [1,4], Piotr Martyniuk [1,5] and Hailu Wang [1,4,*]

[1] State Key Laboratory of Infrared Physics, Shanghai Institute of Technical Physics, Chinese Academy of Sciences, Shanghai 200083, China; zzxykeyan@whut.edu.cn (Z.Z.); 23111110097@stu.xidian.edu.cn (M.K.); fangyueyue22@mails.ucas.ac.cn (Y.F.); piotr.martyniuk@wat.edu.pl (P.M.)
[2] School of Material Science and Engineering, Wuhan University of Technology, Wuhan 430070, China
[3] State Key Discipline Laboratory of Wide Band Gap Semiconductor Technology, School of Microelectronics, Xidian University, 2 South Taibai Road, Xi'an 710071, China
[4] University of Chinese Academy of Sciences, Beijing 100049, China
[5] Institute of Applied Physics, Military University of Technology, 2 Kaliskiego St., 00-908 Warsaw, Poland
* Correspondence: wanghailu@mail.sitp.ac.cn
† These authors contributed equally to this work.

Abstract: The avalanche multiplication effect, capable of significantly amplifying weak optical or electrical signals, plays a pivotal role in enhancing the performance of electronic and optoelectronic devices. This effect has been widely employed in devices such as avalanche photodiodes, impact ionization avalanche transit time diode, and impact ionization field-effect transistors, enabling diverse applications in biomedical imaging, 3D LIDAR, high-frequency microwave circuits, and optical fiber communications. However, the evolving demands in these fields require avalanche devices with superior performance, including lower power consumption, reduced avalanche threshold energy, higher efficiency, and improved sensitivity. Over the years, significant efforts have been directed towards exploring novel device architectures and multiplication mechanisms. The emergence of two-dimensional (2D) materials, characterized by their exceptional light-matter interaction, tunable bandgaps, and ease of forming junctions, has opened up new avenues for developing high-performance avalanche devices. This review provides an overview of carrier multiplication mechanisms and key performance metrics for avalanche devices. We discuss several device structures leveraging the avalanche multiplication effect, along with their electrical and optoelectronic properties. Furthermore, we highlight representative applications of avalanche devices in logic circuits, optoelectronic components, and neuromorphic computing systems. By synthesizing the principles and applications of the avalanche multiplication effect, this review aims to offer insightful perspectives on future research directions for 2D material-based avalanche devices.

Keywords: two-dimensional materials; avalanche multiplication effect; avalanche photodiodes; impact ionization field-effect transistors; neuromorphic devices

Academic Editor: Mircea Dragoman

Received: 3 March 2025
Revised: 10 April 2025
Accepted: 19 April 2025
Published: 22 April 2025

Citation: Zhou, Z.; Kang, M.; Fang, Y.; Martyniuk, P.; Wang, H. Avalanche Multiplication in Two-Dimensional Layered Materials: Principles and Applications. *Nanomaterials* **2025**, *15*, 636. https://doi.org/10.3390/nano15090636

1. Introduction

The avalanche multiplication effect refers to a carrier multiplication process where high-energy electrons or holes initiate impact ionization, generating numerous secondary electron-hole pairs. This cascade effect produces substantial signal amplification of weak optical or electrical inputs [1–3], making it particularly valuable for enhancing the performance in electronic and optoelectronic devices including avalanche photodiodes (APDs)

and impact ionization field-effect transistors (IIFETs). With ongoing technological advancements, avalanche devices based on traditional semiconductor materials, including silicon [4], germanium [5], InGaAs [6,7], HgCdTe [8], and type-II superlattices [9], have developed into a comprehensive technological system.

In an avalanche device, the minimum threshold energy required for avalanche breakdown is approximately equal to the semiconductor's bandgap energy ($E_{thre} \approx E_g$) [10–12]. However, in conventional semiconductor materials, the carrier multiplication process exhibits low efficiency and requires significantly higher threshold energies—typically 22 times greater than the bandgap energy. This inefficiency arises from two primary factors: the limited density of final states due to momentum conservation constraints and the rapid energy dissipation of carriers through phonon scattering. Consequently, conventional bulk-material avalanche devices require high external bias voltages (typically >100 V for Si and >40 V for InGaAs devices) to initiate impact ionization and sustain avalanche multiplication [13–15]. While these devices achieve excellent electrical and optoelectronic performance, the high operating voltages lead to three fundamental limitations: (1) elevated power consumption, (2) increased device noise that degrades the signal-to-noise ratio (SNR), and (3) the need for expensive high-voltage readout circuitry. These factors collectively constrain their applications in low-power electronics and high-SNR optoelectronics [16–18]. In response, researchers have begun exploring novel device structures and multiplication mechanisms to overcome these limitations.

In recent years, breakthroughs in large-scale material growth and integration technologies have enabled significant advances in high-performance electronics and optoelectronics [19–21]. Among the emerging materials, two-dimensional (2D) materials have garnered considerable attention due to their exceptional mechanical flexibility, strong light-matter interaction, and layer-dependent band structures [22–27]. Unlike bulk materials, 2D materials exhibit unique quantum confinement effects that relax the strict momentum conservation requirements, which can significantly influence carrier thermalization processes [28–30]. This modified thermalization behavior directly competes with the carrier multiplication mechanism, potentially altering the overall avalanche characteristics [31,32]. This unique property enables carriers to gain sufficient energy for avalanche multiplication at significantly lower voltages, thereby drastically reducing power consumption while simultaneously enhancing sensitivity and noise performance [33–35].

In this review, we begin by examining the carrier multiplication mechanism and key performance metrics, followed by a detailed demonstration of typical device structures that leverage the avalanche multiplication effect, along with their corresponding electrical and optoelectronic properties. Additionally, we highlight representative applications of the avalanche multiplication effect, including high-sensitivity photodetection, complementary logic inverters, low-power transistors, and neuromorphic computing devices. Through a systematic integration of fundamental mechanisms and practical implementations, this review aims to offer fresh perspectives to propel the development of next-generation 2D avalanche devices.

2. Mechanism and Properties of Avalanche Multiplication Effect

The avalanche multiplication effect of charge carriers is the core working principle of avalanche devices, as illustrated in Figure 1a. In optoelectronic devices, when the photon energy exceeds the bandgap energy of the semiconductor material, the photon energy can be absorbed by electrons, transitioning them to the excited state energy level of the conduction band. At this stage, the electron temperature exceeds the lattice, earning them the designation of "hot electrons". These hot electrons rapidly release their excess energy and go back to the bottom of the conduction band through phonon scattering processes.

If the excess energy surpasses the material's bandgap, electrons in the valence band can be excited into the conduction band by energy exchange with the hot electrons, thereby achieving carrier multiplication [36–38].

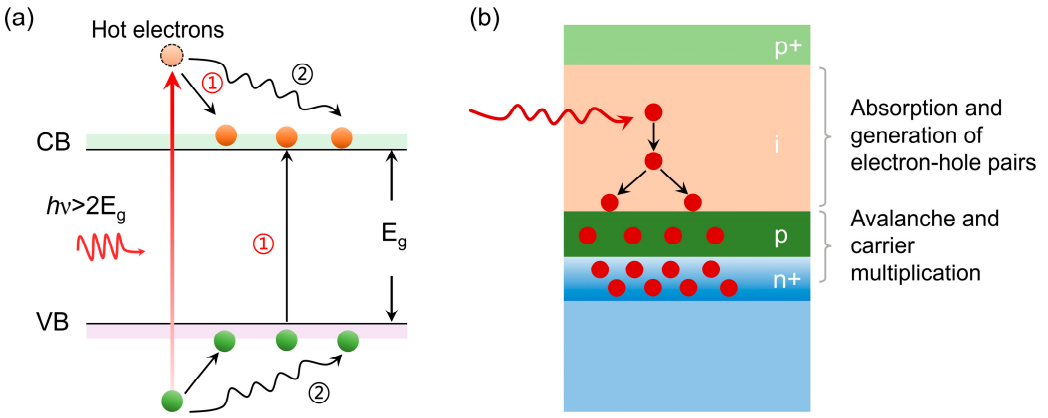

Figure 1. Avalanche multiplication mechanism. (**a**) Carrier multiplication processes in semiconductor devices. Processes ① and ② correspond to carrier multiplication and hot carrier cooling through phonon emission, respectively. (**b**) Impact ionization and multiplication process in avalanche diode structures.

When a strong external bias electric field is applied to the semiconductor material, carriers gain sufficient energy to generate additional electron-hole pairs via continuous impact ionization. The newly generated charge carriers are also accelerated by the electric field, leading to the continuous production of more charge carriers and the manifestation of the avalanche effect. This process facilitates carrier multiplication through impact ionization, whereby an initial few charge carriers generate a substantial cascade, dramatically enhancing current flow. As a result, avalanche devices can detect weak signals that are beyond the reach of traditional photodetectors, providing high sensitivity to low-intensity light signals. This capability makes avalanche devices particularly valuable for applications requiring the detection of faint optical signals [39,40].

The multiplication factor or avalanche gain (M) is one of the important indicators of avalanche devices, which can reflect the device's ability to amplify the photocurrent. It is defined as the ratio of the final output photogenerated current to the photogenerated current before multiplication and can be expressed as [41]:

$$M = \frac{I_p - I_d}{I_{p0} - I_{d0}} \tag{1}$$

where I_p and I_d are the light/dark currents after multiplication, and I_{p0} and I_{d0} are the light/dark currents before multiplication. The higher M is, the better the detector's ability to amplify the optical signal.

Excess noise arises from the stochastic nature of carrier impact ionization during the avalanche multiplication process, presenting significant challenges for the development of accurate theoretical models. Recently, the Hu-Xie avalanche theory was introduced, utilizing a first-principles approach to establish a parameter-free analytical model [42]. This model fundamentally explains the anomalous noise suppression in HgCdTe based on quantum mechanics, playing a pivotal role in advancing avalanche devices. As emphasized by Markus in his recent review, the Hu-Xie theory represents a groundbreaking paradigm

for device optimization and noise suppression [43]. The excess noise factor $F(M)$ is used to characterize the gain instability, which can be expressed as [44]:

$$F(M) = \frac{\langle M^2 \rangle}{\langle M \rangle^2} \tag{2}$$

Based on the local collisional ionization model proposed by McIntyre, the ionization coefficients α and β for electrons and holes are solely dependent on the electric field. These coefficients are defined as the number of times carriers undergo collisional ionization per unit distance. Specifically, the ratio k of the ionization coefficients is given by:

$$k = \frac{\alpha}{\beta} \tag{3}$$

Since $F(M)$ is only related to k for a certain gain, it can be expressed as:

$$F(M) = kM + (1 - k)(2 - \frac{1}{M}) \tag{4}$$

When M is determined, $F(M)$ decreases as k decreases. This provides a theoretical basis for the structural design and material selection of low-noise avalanche devices by increasing (or suppressing) the collision ionization of a carrier, resulting in a decrease in k value and thus reducing $F(M)$. Due to the constraints imposed by material properties (α and β) on the ionization coefficient ratio (k), when both electrons and holes undergo impact ionization ($k \to 1$), charge carriers separate under the electric field, leading to bidirectional carrier transport and chain-reaction avalanche multiplication. In contrast, when $k \to 0$, only electrons (or holes) contribute significantly to the multiplication process, enabling comparable gain within a shorter timescale due to unipolar carrier transport. Therefore, by strategically selecting materials that favor single-carrier multiplication (either electrons or holes), avalanche devices can achieve deterministic gain with minimal excess noise.

3. Typical Device Structures Based on the Avalanche Multiplication Effect

Traditional material-based avalanche devices exhibit fundamental limitations including elevated power requirements and significant noise generation. In contrast, 2D materials offer an attractive alternative platform due to their monolayer thickness and tunable electronic characteristics. The strong quantum size effect resulting from this nanoscale thickness significantly enhances Coulomb interactions, which greatly facilitates energy exchange between charge carriers, thereby enabling efficient avalanche multiplication [45–47]. Additionally, 2D materials exhibit higher exciton binding energy and lower electron-phonon coupling efficiency compared to bulk materials, leading to longer carrier lifetimes [48]. These unique physical properties allow 2D material-based avalanche devices to trigger avalanche multiplication effects at significantly lower bias voltages, paving the way for the development of high-gain, low-noise avalanche devices. Therefore, extensive research has been conducted in this field. Table 1 summarizes the performance parameters of avalanche detectors based on typical bulk materials and 2D materials. The compared metrics include responsivity (R), response time (RT), operating wavelength (λ), dark current (I_{Dark}), multiplication factor (M), operating temperature (T), threshold voltage, and external quantum efficiency (EQE). While conventional bulk-material avalanche devices exhibit robust performance at room temperature, they inherently require high breakdown voltages (exceeding 30 V). In comparison, two-dimensional material-based devices achieve lower operational voltages due to their small size but often operate with slow response time and low responsivity. Below, we provide a detailed classification and analysis of these structures to better understand their design principles and performance characteristics.

3.1. Schottky Junction

When metals come into contact with semiconductor materials, potential barriers are typically formed at the interface due to differences in their work functions (Figure 2a) [49,50]. These barriers can effectively block dark charge carriers during avalanche processes, enabling the realization of avalanche devices with high gain and reduced noise [51]. Inspired by this concept, X. Li et al. demonstrated the use of work function matching in WSe_2 devices to address the inherent gain-noise issue in the process of avalanche multiplication [52]. By strategically designing Schottky barriers, they achieved a significant reduction in noise while maintaining high gain, showcasing a promising approach for optimizing the performance of 2D material-based avalanche devices. As illustrated in Figure 2e, when a high reverse bias is applied, the photogenerated carriers are sufficiently accelerated to initiate the avalanche multiplication effect at a lower electric field, while dark carriers are blocked by the Schottky barriers at the platinum contact. This approach achieves a remarkable gain of 5×10^5, while the noise equivalent power is reduced to 8.09 $fW/Hz^{1/2}$, as shown in Figure 2i, thereby offering a novel perspective for detecting weak signals. Similarly, J. Jia et al. demonstrated avalanche carrier multiplication through the Schottky barrier formed by the Ti/black phosphorus (BP) contact [53]. Their findings indicate that the 2D BP device achieves an external quantum efficiency (EQE) of 310 and a responsivity of 130 A/W, while attaining a signal-to-noise ratio of 100 dB. Additionally, Z. Zhang et al. reported comparable results using a Schottky barrier formed by graphite/InSe with low threshold voltage, but unlike conventional avalanche devices, it exhibits a negative temperature coefficient [54].

3.2. Stepwise Junction

J. Kim et al. identified that phonons in transition metal dichalcogenides (TMDs) can be categorized into two modes: in-plane and out-of-plane [39], through testing the carrier multiplication efficiency in thinned WSe_2 and $MoTe_2$ materials. Generally, the out-of-plane mode is more active in electron-phonon (e-p) interactions than the in-plane mode, and the contribution of the out-of-plane mode to e-p scattering can be significantly diminished by reducing the material thickness. According to this discovery, by thinning a portion of a 2D material and shaping it into a stepwise structure with few/multiple layers acting as wide/narrow gap semiconductors, the avalanche process of charge carriers can be triggered earlier. H. Wang et al. utilized mechanical exfoliation technology to fabricate WSe_2 into the structure illustrated in Figure 2b [55]. In this structure, the pristine homojunction interface eliminates detrimental scattering induced by interface defect states. Meanwhile, the stepwise morphology induces strong localized electric fields that enhance Coulomb interactions between charge carriers while suppressing out-of-plane phonon-mode-dominated scattering processes. This enables the achievement of a threshold energy approaching the theoretical limit E_g (where E_g is the semiconductor bandgap) at room temperature. The device exhibits an extremely low dark current (10–100 fA) and achieves detection sensitivity up to 10,000-photon level in the near-infrared range. Recently, the same group further developed an IIFET based on a stepwise van der Waals WSe_2 homojunction. The fabricated device demonstrates a low subthreshold swing (SS) of 3.09 mV/dec and a high multiplication factor exceeding 10^4 at room temperature [56]. These works provides new perspectives for developing next-generation avalanche devices with high sensitivity, low power consumption, and low threshold voltage.

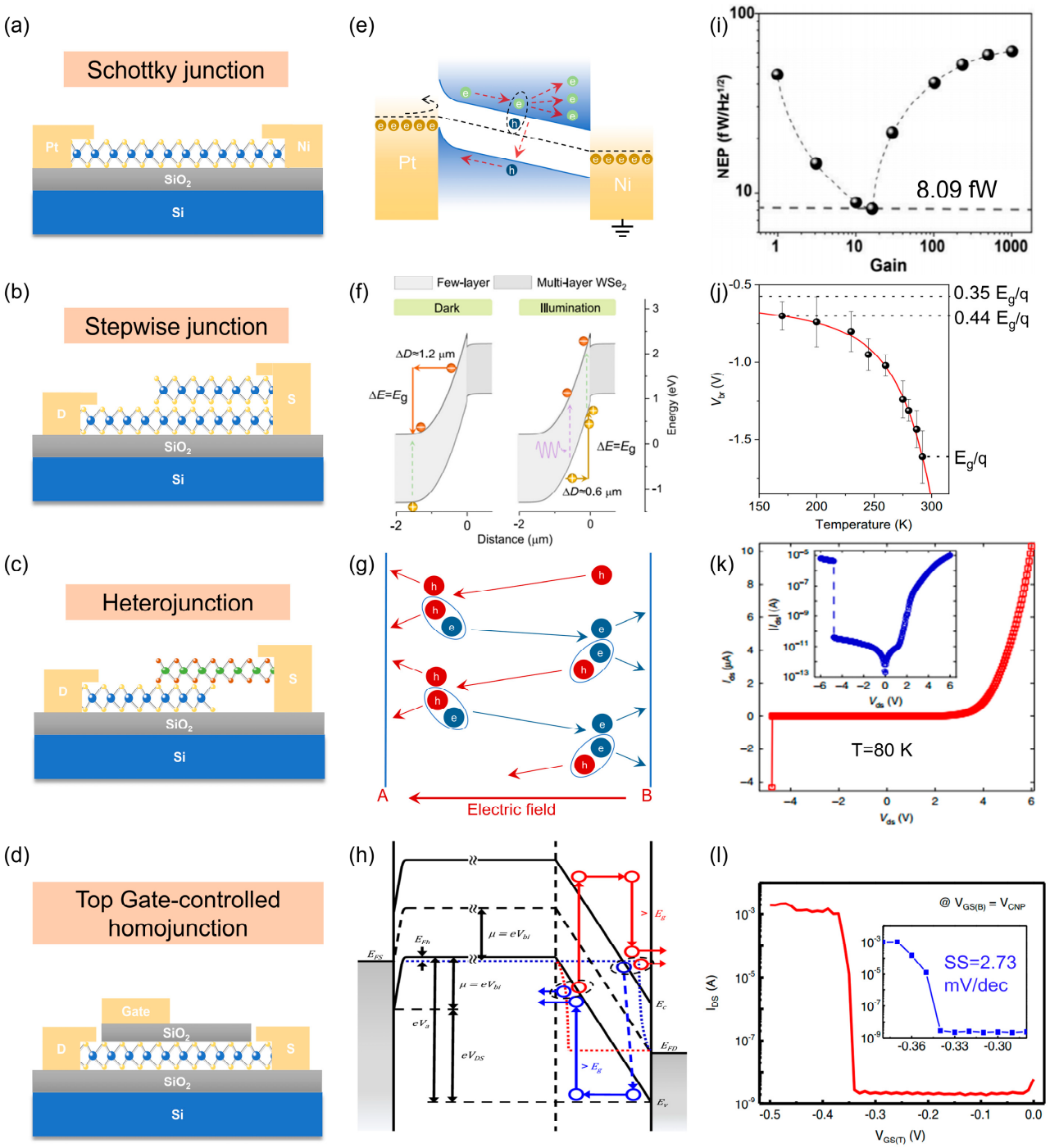

Figure 2. Working principles and performance characteristics of avalanche devices with different structures. (**a**–**d**) Structural models of Schottky junction, stepwise junction, heterojunction, and top gate-controlled homojunction, respectively. Schottky junctions typically employ metals with large work function contrasts, e.g., Pt (~5.65 eV) and Ni (~4.6 eV). (**e**–**h**) Working principles of Pt/Wse_2/Ni Schottky junction, WSe_2 stepwise junction, InSe/BP heterojunction, and WSe_2 top gate-controlled homojunction, respectively. (**i**) NEP curves of Pt/WSe_2/Ni Schottky junction. (**j**) Reverse breakdown voltage versus operating temperature curve of WSe_2 stepwise junction. (**k**) I_{DS}-V_{DS} curves of InSe/BP heterojunction. (**l**) Enlarged view of the I_{DS}-V_{GS} characteristics and subthreshold region of the WSe_2 top gate-controlled homojunction at room temperature.

3.3. Heterojunction

When two distinct semiconductors are brought into contact, the application of a relatively small bias voltage can induce significant band bending at the material interface. This band bending enables photogenerated carriers to acquire sufficient energy to trigger avalanche gain at a much lower bias voltage compared to traditional semiconductors [57–59]. To achieve a device characterized by high gain, low bias, and low noise, A. Gao et al. constructed a vertical InSe/BP heterojunction structure that leverages the ballistic avalanche phenomenon [60]. This design results in a detector with a low avalanche threshold voltage (approximately 4.8 V) and outstanding noise characteristics. As illustrated in Figure 2g, conventional avalanche devices rely on a cascade process for rapid current multiplication, which generates significant excess noise due to the random generation of carriers. In contrast, the ballistic avalanche process occurs within a nanoscale transport channel, where a hole is energized sufficiently by the electric field to create an electron-hole pair in Region A. Simultaneously, two holes are collected, and electrons are injected back into the channel, initiating a shock ionization process that generates another electron-hole pair in Region B. At this stage, two electrons are collected, and the hole triggers the avalanche process anew. The symmetric energy band structure of BP ensures that the ionization probabilities for electrons and holes are equal, facilitating substantial carrier multiplication without inducing excess noise during the ballistic avalanche process, as no scattering events occur.

For WSe_2/MoS_2 two-photon absorbing heterojunctions, B. Son et al. achieved avalanche multiplication of electrons and holes in WSe_2 and MoS_2 monolayers [57], respectively, by applying a moderate bias of >6.5 V. The ultrahigh gain of approximately 1300 enhanced the device's responsivity by nearly three orders of magnitude, reaching 88 μA/W. This work paves the way for the development of photonic integrated circuits and presents new possibilities for the construction of practical infrared detectors.

3.4. Top Gate-Controlled Homojunction

To achieve the goals of low power consumption and high energy efficiency, reducing the subthreshold swing has emerged as a critical research focus [61–64]. This effort has spurred extensive investigations, as summarized in Table 2, which provides detailed performance metrics including the subthreshold swing, the ratio of on-state current to off-state current (on/off ratio), on-state current density (I_{on}), and off-state current density (I_{off}). Among these efforts, leveraging the impact ionization mechanism to harness the high-gain characteristics of avalanche breakdown has emerged as an effective strategy for minimizing energy consumption in device operation [65,66]. By employing top-gate modulation on homogeneous WSe_2 transverse junctions, H. Choi et al. demonstrated exceptional performance, achieving an average SS as low as 2.73 mV/dec and reducing the device's threshold voltage to below 1 V [67]. Specifically, in the region covered by the top gate, the doping level increases significantly with the application of top-gate voltage, eventually leading to the metallization of this area and effectively shortening the channel length. Simultaneously, in the region without top-gate coverage, the electric field strength is substantially enhanced, enabling carriers to gain sufficient energy to generate electron-hole pairs through impact ionization, thereby facilitating carrier multiplication. This mechanism not only significantly improves the device's switching characteristics but also provides a novel pathway for the design of energy-efficient electronic devices.

Table 1. Performance metrics of bulk and two-dimensional material avalanche devices with different structures.

Structures		Device	*R* (A/W)	*RT* (ms)	*λ* (nm)	I_{Dark} (A)	*M*	*T* (K)	Threshold Voltage (V)	*EQE* (%)	Ref.
Bulk materials		Si	50–120	$0.1–2 \times 10^{-6}$	400–1100	$0.1–1 \times 10^{-9}$	20–400	300	150–400	77	[4]
		Ge	2.5–25	$5–8 \times 10^{-7}$	800–1650	$5–50 \times 10^{-8}$	50–200	/	20–40	55–75	[5]
		InGaAs	/	$1–5 \times 10^{-7}$	1100–1700	$1–5 \times 10^{-8}$	10–40	/	20–30	60–70	[6]
Two-dimensional materials	Schottkyjunction	WSe_2	/	0.05	520	10^{-14}	5×10^5	300	15	60	[52]
		$MoTe_2$-WS_2-$MoTe_2$	6.02	475	400–700	9.3×10^{-11}	587	295	10.4	1406	[49]
		InSe	11,000	1	405–785	5×10^{-9}	500	/	1.3	/	[50]
		BP	130	/	500–1100	2×10^{-6}	7	300	14.7	31,000	[53]
		InSe	/	0.06	400–800	1.3×10^{-9}	152	/	12	866	[51]
	Stepwise junction	WSe_2	/	/	520	1×10^{-15}	470	300	1.6	/	[55]
		WSe_2	/	/	/	/	10^4	300	4	/	[56]
	Heteroj-unction	WSe_2/MoS_2	8.8×10^{-5}	/	532–1030	/	1300	300	6.5	/	[57]
		Gr-$MoTe_2$-Gr	5	0.03	600–1350	/	/	300	/	40	[58]
		Gr-$MoTe_2$-Gr	0.03	6.15×10^{-3}	550	6×10^{-8}	/	300	/	/	[59]
		BP/InSe	80	/	4000	/	10^4–10^5	10–180	4.8	2480	[60]
	Top Gate-controlled homojunction	WSe_2	/	/	/	/	106	300	0.88	/	[67]

Note. *R*: responsivity; *RT*: response time; *λ*: wavelength; I_{Dark}: dark current; *M*: multiplication factor; *T*: temperature; *EQE*: external quantum efficiency; BP: black phosphorus; Gr: graphene.

Table 2. Comparison of the key performance metrics in 2D material-based IIFETs.

Device	Subthreshold Swing (mV/dec)	On/Off Ratio	I_{on}	I_{off}	Ref.
WSe_2	2.73	10^6	2.29×10^{-3} A	1×10^{-9} A	[67]
MoS_2	0.7	10^7	10^{-6} A/μm	10^{-13}A/μm	[61]
Gr/InAs	<0.6	10^6	2.3×10^{-4} A/μm	/	[65]
MoS_2	11	10^6	10^{-6} A	10^{-12} A	[62]
Gr/BP/InSe	0.4	$>10^5$	1×10^{-6} A/μm	1.2×10^{-11}A/μm	[66]
MoS_2	2.5	10^6	5.4×10^{-6} A/μm	1×10^{-12}A/μm	[63]
InSe/BP	<0.25	10^4	1×10^{-6} A	1.64×10^{-10} A	[60]
MoS_2	2.26	10^6	3.9×10^{-6} A	1.9×10^{-12} A	[64]
WSe_2	3.09	$>10^5$	1×10^{-6} A/μm	/	[56]

4. Application of Avalanche Multiplication

The avalanche effect, leveraging its unique carrier multiplication mechanism, plays a pivotal role in advancing multiple frontier technologies. In optoelectronic detection, APDs provide substantial signal amplification, enabling high-sensitivity detection of weak optical signals. Silicon-based APDs, utilizing wide-bandgap semiconductor materials, achieve efficient visible-light detection, while InGaAs/InP heterostructure devices—with a spectral response spanning 0.7–1.6 μm—serve as the cornerstone for extending detection capabilities in long-haul fiber-optic communications [68,69]. Beyond telecommunications, the avalanche effect is instrumental in LiDAR systems, where it facilitates the detection of low-reflectivity objects and enables high-resolution 3D imaging for autonomous driving applications. In high-frequency electronics, avalanche transit-time diodes (IMPATT diodes) exploit the interplay between impact ionization and carrier transit-time delay to generate millimeter-wave and terahertz signals, making them vital for next-generation wireless and sensing technologies [2,70]. The biomedical field also benefits from avalanche-based detectors, such as APDs and single-photon avalanche diode (SPAD) arrays, which enhance fluorescence-based imaging, surgical navigation, and high-resolution tomography [71,72]. However, the growing demands of artificial intelligence—particularly in computational imaging and edge sensing—pose new challenges for avalanche devices in terms of speed,

noise performance, and integration density. This section will examine recent progress in avalanche-effect applications across these pioneering fields, with particular emphasis on performance optimization strategies and emerging hybrid architectures.

As the integration density of transistors on a single chip continues to increase, power consumption has become a critical challenge. To minimize the power consumption of individual transistors, it is essential to achieve the lowest possible SS, enabling rapid switching between the "0" and "1" states. H. Choi et al. demonstrated this principle using a complementary inverter composed of p-type WSe_2 and n-type MoS_2 connected in series [67]. This complementary inverter dynamically adjusts the output signal state based on the input signal level. When the input voltage (V_{in}) is high, the electron-dominated characteristics of n-type MoS_2 pull the output voltage (V_{out}) low. Conversely, when V_{in} is low, the hole impact ionization in p-type WSe_2 drives the V_{out} high. The exceptional subthreshold swing of the WSe_2 device allows the complementary inverter to achieve a low switching threshold voltage, as illustrated in Figure 3c,d, and a high inverter gain of approximately 73. Additionally, this study highlights that adjusting device parameters can yield different threshold voltages, making these devices highly adaptable for practical circuit applications. Similarly, B. Yuan et al. developed vertical layered semiconductor field-effect transistor (VSFET) devices with outstanding subthreshold swing [73], achieving a voltage gain of up to 311 at a 2 V supply voltage by integrating a p-type MOSFET with an n-type VSFET configured as a complementary phase shifter. These advancements underscore the potential of leveraging 2D materials for low-power, high-performance electronic devices.

As artificial neural networks continue to advance, their architectures are becoming increasingly complex, leading to higher power consumption. Consequently, avalanche devices with steep SS have attracted considerable attention. By leveraging the high-energy spikes generated by impact ionization during transient time and the ability to control these spikes through operating voltage, these devices can achieve ultra-low power consumption via low operating voltages and fast response times. Furthermore, when integrated with advanced algorithms, they enable energy-efficient neural networks capable of performing complex tasks such as computation and recognition. As shown in Figure 4a, H. Choi et al. employed 2D WSe_2 shock transistors as synapses in conjunction with 2D ferroelectric transistor neurons to construct a neural network [74], achieving remarkably low energy consumption of 2 pJ per single pulse. Additionally, through the synergistic processing capabilities of these components, an accuracy of 87.5% in face classification was achieved after 20 learning sessions using unsupervised learning. Moreover, the MoS_2/WSe_2 heterojunction developed by L. Li et al. demonstrated ultrafast dark and light adaptation processes of 108 μs and 268 μs, respectively, facilitated by the avalanche effect, with switching behavior controlled by the top gate voltage [75]. When combined with deep learning techniques from convolutional neural networks, this system achieved over 98% image recognition accuracy under both dim and bright conditions, as illustrated in Figure 4f,g. These results highlight the significant potential of avalanche photodetectors in the field of bionics, paving the way for energy-efficient and high-performance neuromorphic computing systems.

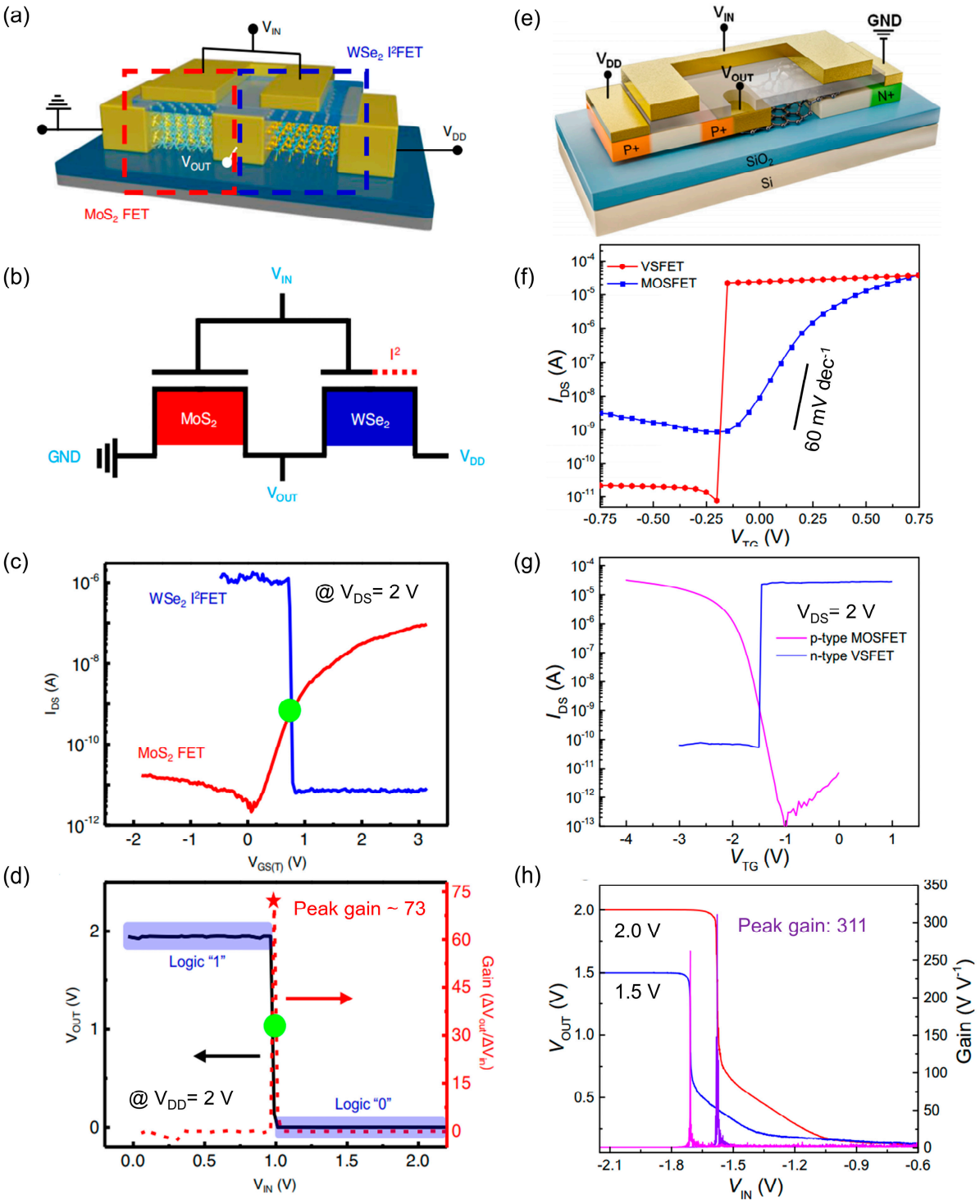

Figure 3. Principles and characteristics of complementary inverter. (**a**,**b**) Structure and schematic diagrams of the complementary inverter based on WSe_2. (**c**) I_{DS}-V_{GS} characteristic curves of WSe_2 and MoS_2 devices. (**d**) Operating characteristic curves of the complementary inverter based on WSe_2 in series with MoS_2 device. The star indicates that the device achieved a high inverter gain of approximately 73. (**e**) Schematic of the structure of the VSFET-based complementary inverter. (**f**) Transfer characteristic curves of the VSFET versus the MOSFET at V_{DS} = 3 V, where the VSFET exhibits excellent SS. (**g**) Transfer characteristic curves of the VSFET versus the MOSFET during complementary inverter operation. (**h**) Voltage transfer characteristic and gain of the inverter.

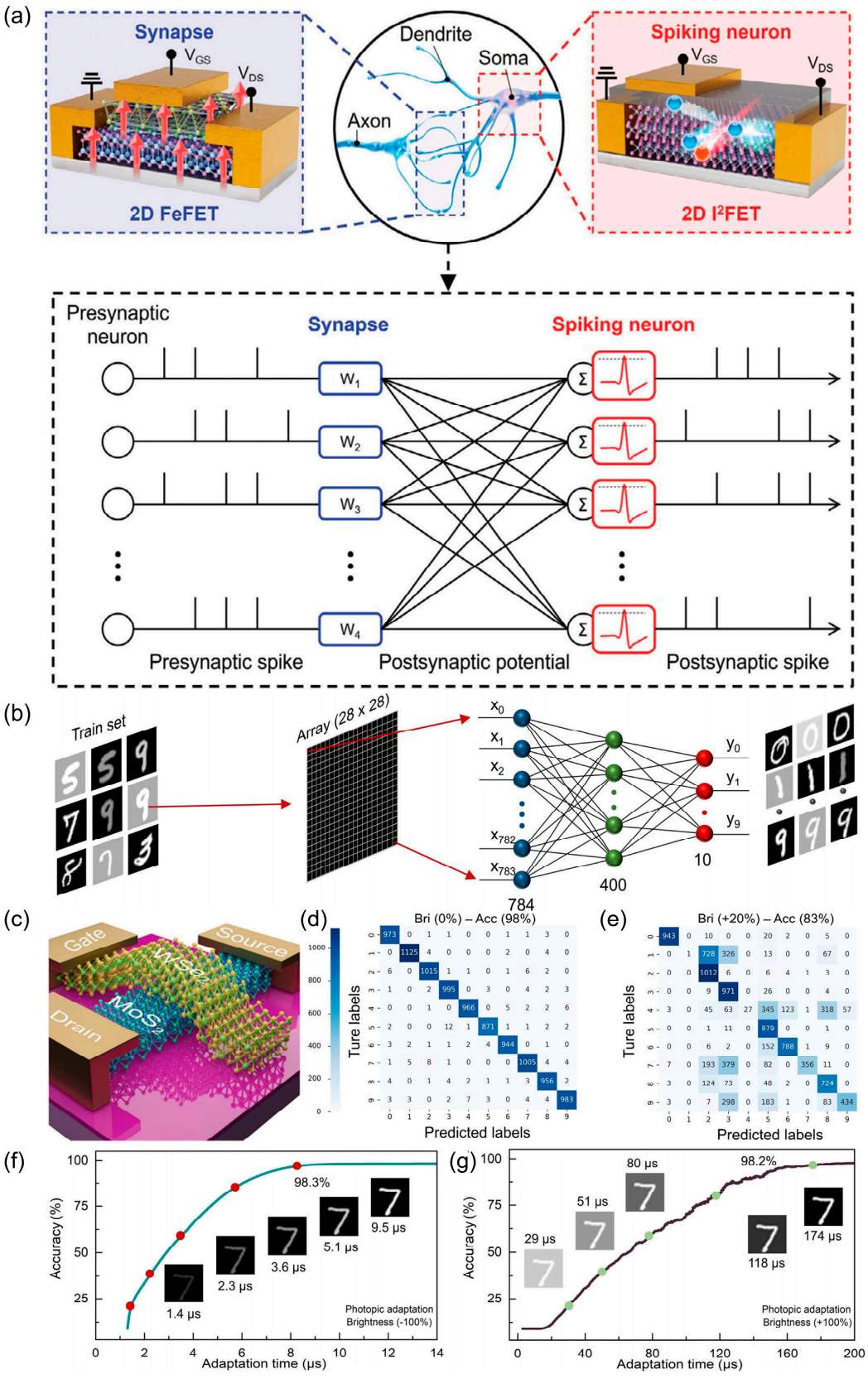

Figure 4. Neuromorphic computing systems. (**a**) Schematic of the peak neural network structure and framework. (**b**) Machine vision image recognition based on convolutional neural networks. (**c**) Diagram of adaptive machine vision device. (**d**) Confusion matrix and its recognition accuracy at standard vs. (**e**) +20% luminance. (**f**,**g**) Recognition rate as a function of time for adaptive machine vision for (**f**) darkness and (**g**) lightness adaptation.

5. Conclusions

Avalanche devices based on traditional semiconductor materials have achieved industrialization and are widely utilized across various fields. However, as technology continues to advance, emerging applications such as low-power artificial neural networks, bionic vision, and low-light detection have imposed higher performance demands on detectors. In this context, avalanche devices based on 2D materials have rapidly evolved, demonstrating exceptional performance in sensitivity, response time, and power consumption. In this review, we provide a concise introduction to the avalanche multiplication mechanism and its key performance metrics, followed by a detailed discussion of the typical structures and applications of 2D material-based avalanche devices. By synthesizing these insights, we aim to offer valuable guidance for the development of more advanced and efficient avalanche devices in the future.

Author Contributions: Z.Z. and M.K. contributed equally to this work; H.W. supervised the project and developed the review ideas; Z.Z. and M.K. conducted extensive research on the relevant content covered in the review; Z.Z., M.K. and Y.F. organized the data covered in the relevant literature; Z.Z. and M.K. wrote the manuscript and visualized the content; P.M. reviewed the manuscript, discussed and elaborated on the logical and physical mechanisms involved, and assisted Z.Z. and M.K. with the formatting; H.W. planned and staffed the entire process of writing the manuscript. All authors have read and agreed to the published version of the manuscript.

Funding: This work was supported by the National Natural Science Foundation of China (Grant No. 62304231), National Science Centre (NCN) and the National Natural Science Foundation of China (NSFC) "SHENG 3" UMO-2023/48/Q/ST7/00144 (NCN) and 62361136587 (NSFC), China National Postdoctoral Program for Innovative Talent (Grant No. BX20230390), Shanghai Science and Technology Committee (Grant Nos. 23YF1455400 and 23xtcx00300), and China Postdoctoral Science Foundation (Grant No. 2023M733622).

Conflicts of Interest: The authors declare no conflicts of interest.

References

1. Zhang, Q.Y.; Li, N.; Zhang, T.; Dong, D.M.; Yang, Y.T.; Wang, Y.H.; Dong, Z.A.; Shen, J.Y.; Zhou, T.H.; Liang, Y.L.; et al. Enhanced gain and detectivity of unipolar barrier solar blind avalanche photodetector via lattice and band engineering. *Nat. Commun.* **2023**, *14*, 418. [CrossRef] [PubMed]
2. Izhnin, I.I.; Lozovoy, K.A.; Kokhanenko, A.P.; Khomyakova, K.I.; Douhan, R.M.H.; Dirko, V.V.; Voitsekhovskii, A.V.; Fitsych, O.I.; Akimenko, N.Y. Single-photon avalanche diode detectors based on group IV materials. *Appl. Nanosci.* **2022**, *12*, 253–263. [CrossRef]
3. Bartolo-Perez, C.; Chandiparsi, S.; Mayet, A.S.; Cansizoglu, H.; Gao, Y.; Qarony, W.; AhAmed, A.; Wang, S.Y.; Cherry, S.R.; Islam, M.S.; et al. Avalanche photodetectors with photon trapping structures for biomedical imaging applications. *Opt. Express* **2021**, *29*, 19024–19033. [CrossRef] [PubMed]
4. Hamamatsu S12023 Series. Available online: https://www.hamamatsu.com.cn/cn/zh-cn/product/optical-sensors/apd/si-apd/S12023-02.html (accessed on 10 October 2024).
5. Ushio PDGAJ Series. Available online: https://www.ushio.com/product/pd-ld-germanium-avalanche-photodiode/ (accessed on 4 June 2020).
6. Hamamatsu G8931 Series. Available online: https://www.hamamatsu.com.cn/cn/zh-cn/product/optical-sensors/apd/ingaas-apd/G8931-04.html (accessed on 10 July 2024).
7. Shi, Z.W.; Ke, S.Y.; Meng, W.H.; Wang, Z.R.; Guo, M.H.; Jiang, X.L.; Liu, K.; Lin, Z.W.; Chen, X.P. Double modulation of the electric field in InGaAs/Si APD by groove rings for the achievement of THz gain-bandwidth product. *Phys. Scr.* **2024**, *99*, 115501. [CrossRef]
8. Zhu, L.Q.; Ge, H.C.; Guo, H.J.; Chen, L.; Lin, C.; Chen, B.L. Gain and Excess Noise in HgCdTe e-Avalanche Photodiodes at Various Temperatures and Wavelengths. *IEEE Trans. Electron Devices* **2023**, *70*, 2384–2388. [CrossRef]
9. Yan, S.L.; Huang, J.; Zhang, Y.; Ma, W. Mid wavelength type II InAs/GaSb superlattice avalanche photodiode with AlAsSb multiplication layer. *IEEE Electron Device Lett.* **2021**, *42*, 1634–1637. [CrossRef]

10. Gatt, P.; Johnson, S.; Nichols, T. Geiger-mode avalanche photodiode ladar receiver performance characteristics and detection statistics. *Appl. Opt.* **2009**, *48*, 3261–3276. [CrossRef]
11. Albota, M.A.; Heinrichs, R.M.; Kocher, D.G.; Fouche, D.G.; Player, B.E.; O'Brien, M.E.; Aull, B.F.; Zayhowski, J.J.; Mooney, J.; Willard, B.C.; et al. Three-dimensional imaging laser radar with a photon-counting avalanche photodiode array and microchip laser. *Appl. Opt.* **2002**, *41*, 7671–7678. [CrossRef]
12. Kardynal, B.E.; Yuan, Z.L.; Shields, A.J. An avalanche-photodiode-based photon-number-resolving detector. *Nat. Photonics* **2008**, *2*, 425–428. [CrossRef]
13. Kang, Y.M.; Liu, H.D.; Morse, M.; Paniccia, M.J.; Zadka, M.; Litski, S.; Sarid, G.; Pauchard, A.; Kuo, Y.H.; Chen, H.W.; et al. Monolithic germanium/silicon avalanche photodiodes with 340 GHz gain-bandwidth product. *Nat. Photonics* **2009**, *3*, 59–63. [CrossRef]
14. Kim, S.; Myeong, G.; Shin, W.; Lim, H.; Kim, B.; Jin, T.; Chang, S.; Watanabe, K.; Taniguchi, T.; Cho, S. Thickness-controlled black phosphorus tunnel field-effect transistor for low-power switches. *Nat. Nanotechnol.* **2020**, *15*, 203–206. [CrossRef] [PubMed]
15. Wang, Y.; Gu, Y.; Cui, A.L.; Li, Q.; He, T.; Zhang, K.; Wang, Z.; Li, Z.P.; Zhang, Z.H.; Wu, P.S.; et al. Fast Uncooled Mid-Wavelength Infrared Photodetectors with Heterostructures of van der Waals on Epitaxial HgCdTe. *Adv. Mater.* **2022**, *34*, 2107772. [CrossRef] [PubMed]
16. Ahmed, I.; Shi, L.; Pasanen, H.; Vivo, P.; Maity, P.; Hatamvand, M.; Zhan, Y.Q. There is plenty of room at the top: Generation of hot charge carriers and their applications in perovskite and other semiconductor-based optoelectronic devices. *Light-Sci. Appl.* **2021**, *10*, 174. [CrossRef]
17. Li, M.J.; Fu, J.H.; Xu, Q.; Sum, T.C. Slow Hot-Carrier Cooling in Halide Perovskites: Prospects for Hot-Carrier Solar Cells. *Adv. Mater.* **2019**, *31*, e1802486. [CrossRef]
18. Weng, Q.C.; Komiyama, S.; Yang, L.; An, Z.H.; Chen, P.P.; Biehs, S.A.; Kajihara, Y.; Lu, W. Imaging of nonlocal hot-electron energy dissipation via shot noise. *Science* **2018**, *360*, 775–778. [CrossRef]
19. Akinwande, D.; Huyghebaert, C.; Wang, C.H.; Serna, M.I.; Goossens, S.; Li, L.J.; Wong, H.S.P.; Koppens, F.H.L. Graphene and two-dimensional materials for silicon technology. *Nature* **2019**, *573*, 507–518. [CrossRef] [PubMed]
20. Lan, C.Y.; Zhou, Z.Y.; Zhou, Z.F.; Li, C.; Shu, L.; Shen, L.F.; Li, D.P.; Dong, R.T.; Yip, S.P.; Ho, J. Wafer-scale synthesis of monolayer WS_2 for high-performance flexible photodetectors by enhanced chemical vapor deposition. *Nano Res.* **2018**, *11*, 3371–3384. [CrossRef]
21. Guo, N.; Xiao, L.; Gong, F.; Luo, M.; Wang, F.; Jia, Y.; Chang, H.C.; Liu, J.K.; Li, Q.; Wu, Y.; et al. Light-Driven WSe_2-ZnO Junction Field-Effect Transistors for High-Performance Photodetection. *Adv. Sci.* **2020**, *7*, 1901637. [CrossRef]
22. Liu, Y.; Huang, Y.; Duan, X.F. Van der Waals integration before and beyond two-dimensional materials. *Nature* **2019**, *567*, 323–333. [CrossRef]
23. Jariwala, D.; Marks, T.J.; Hersam, M.C. Mixed-dimensional van der Waals heterostructures. *Nat. Mater.* **2017**, *16*, 170–181. [CrossRef]
24. Meng, L.Y.; Zhang, J.M.; Yuan, X.X.; Yang, M.L.; Wang, B.; Wang, L.M.; Zhang, N.N.; Liu, M.L.; Zhu, Z.M.; Hu, H.Y. Gate Voltage Dependence Ultrahigh Sensitivity WS_2 Avalanche Field-Effect Transistor. *IEEE Trans. Electron Devices* **2022**, *69*, 3225–3229. [CrossRef]
25. Meng, L.Y.; Zhang, N.N.; Yang, M.L.; Yuan, X.X.; Liu, M.L.; Hu, H.Y.; Wang, L.M. Low-voltage and high-gain WSe_2 avalanche phototransistor with an out-of-plane WSe_2/WS_2 heterojunction. *Nano Res.* **2023**, *16*, 3422–3428. [CrossRef]
26. Kang, T.; Choi, H.; Li, J.S.; Kang, C.; Hwang, E.; Lee, S. Anisotropy of impact ionization in WSe_2 field effect transistors. *Nano Converg.* **2023**, *10*, 13. [CrossRef] [PubMed]
27. Qiu, W.C.; Hu, W.D. Laser beam induced current microscopy and photocurrent mapping for junction characterization of infrared photodetectors. *Sci. China-Phys. Mech. Astron.* **2015**, *58*, 027001. [CrossRef]
28. Bonaccorso, F.; Sun, Z.; Hasan, T.; Ferrari, A.C. Graphene photonics and optoelectronics. *Nat. Photonics* **2010**, *4*, 611–622. [CrossRef]
29. Xia, F.N.; Wang, H.; Xiao, D.; Dubey, M.; Ramasubramaniam, A. Two-dimensional material nanophotonics. *Nat. Photonics* **2014**, *8*, 899–907. [CrossRef]
30. Hu, W.D.; Chen, X.S.; Ye, Z.H.; Lu, W. A hybrid surface passivation on HgCdTe long wave infrared detector with insitu CdTe deposition and high-density Hydrogen plasma modification. *Appl. Phys. Lett.* **2011**, *99*, 091101. [CrossRef]
31. Wang, Z.; Xia, H.; Wang, P.; Zhou, X.H.; Liu, C.S.; Zhang, Q.H.; Wang, F.; Huang, M.L.; Chen, S.Y.; Wu, P.S.; et al. Controllable Doping in 2D Layered Materials. *Adv. Mater.* **2021**, *33*, 2104942. [CrossRef]
32. Tong, L.; Peng, Z.R.; Lin, R.F.; Li, Z.; Wang, Y.L.; Huang, X.Y.; Xue, K.H.; Xu, H.Y.; Liu, F.; Xia, H.; et al. 2D materials-based homogeneous transistor-memory architecture for neuromorphic hardware. *Science* **2021**, *373*, 1353–1358. [CrossRef]
33. Miao, J.S.; Wang, C. Avalanche photodetectors based on two-dimensional layered materials. *Nano Res.* **2021**, *14*, 1878–1888. [CrossRef]

34. Hu, W.D.; Ye, Z.H.; Liao, L.; Chen, H.L.; Chen, L.; Ding, R.J.; He, L.; Chen, X.S.; Lu, W. 128 x 128 longwavelength/mid-wavelength two-color HgCdle inirared focal plane array detector with ultralow spectral cross talk. *Opt. Lett.* **2014**, *39*, 5184–5187.
35. Wu, P.S.; He, T.; Zhu, H.; Wang, Y.; Li, Q.; Wang, Z.; Fu, X.; Wang, F.; Wang, P.; Shan, C.X.; et al. Next-generation machine vision systems incorporating two-dimensional materials: Progress and perspectives. *Infomat* **2022**, *4*, e12275. [CrossRef]
36. Brongersma, M.L.; Halas, N.J.; Nordlander, P. Plasmon-induced hot carrier science and technology. *Nat. Nanotechnol.* **2015**, *10*, 25–34. [CrossRef]
37. Nozik, A.J. Utilizing hot electrons. *Nat. Energy* **2018**, *3*, 170–171. [CrossRef]
38. Paul, S.; Karak, S.; Mathew, A.; Ram, A.; Saha, S. Electron-phonon and phonon-phonon anharmonic interactions in 2H-MoX_2 (X = S, Te): A comprehensive resonant Raman study. *Phys. Rev. B* **2021**, *104*, 075418. [CrossRef]
39. Kim, J.H.; Bergren, M.R.; Park, J.C.; Adhikari, S.; Lorke, M.; Frauenheim, T.; Choe, D.H.; Kim, B.; Choi, H.; Gregorkiewicz, T.; et al. Carrier multiplication in van der Waals layered transition metal dichalcogenides. *Nat. Commun.* **2019**, *10*, 5488. [CrossRef]
40. Paul, K.K.; Kim, J.H.; Lee, Y.H. Hot carrier photovoltaics in van der Waals heterostructures. *Nat. Rev. Phys.* **2021**, *3*, 178–192. [CrossRef]
41. Shao, Z.G.; Chen, D.J.; Liu, Y.L.; Lu, H.; Zhang, R.; Zheng, Y.D.; Li, L.; Dong, K.X. Significant Performance Improvement in AlGaN Solar-Blind Avalanche Photodiodes by Exploiting the Built-In Polarization Electric Field. *IEEE J. Sel. Top. Quantum Electron.* **2014**, *20*, 3803306. [CrossRef]
42. Xie, R.Z.; Li, Q.; Wang, P.; Chen, X.S.; Lu, W.; Guo, H.J.; Chen, L.; Hu, W.D. Spatial description theory of narrow-band single-carrier avalanche photodetectors. *Opt. Express* **2021**, *29*, 16432–16446. [CrossRef]
43. Liu, S.N.; Han, Q.; Luo, W.J.; Lei, W.; Zhao, J.; Wang, J.; Jiang, Y.D.; Raschke, M.B. Recent progress of innovative infrared avalanche photodetectors. *Infrared Phys. Technol.* **2024**, *137*, 105114. [CrossRef]
44. Zhao, Y.L. Impact Ionization in Absorption, Grading, Charge, and Multiplication Layers of InP/InGaAs SAGCM APDs with a Thick Charge Layer. *IEEE Trans. Electron Devices* **2013**, *60*, 3493–3499. [CrossRef]
45. Gabor, N.M.; Zhong, Z.H.; Bosnick, K.; Park, J.; McEuen, P.L. Extremely Efficient Multiple Electron-Hole Pair Generation in Carbon Nanotube Photodiodes. *Science* **2009**, *325*, 1367–1371. [CrossRef]
46. Brida, D.; Tomadin, A.; Manzoni, C.; Kim, Y.J.; Lombardo, A.; Milana, S.; Nair, R.R.; Novoselov, K.S.; Ferrari, A.C.; Cerullo, G.; et al. Ultrafast collinear scattering and carrier multiplication in graphene. *Nat. Commun.* **2013**, *4*, 1987. [CrossRef]
47. Barati, F.; Grossnickle, M.; Su, S.S.; Lake, R.K.; Aji, V.; Gabor, N.M. Hot carrier-enhanced interlayer electron-hole pair multiplication in 2D semiconductor heterostructure photocells. *Nat. Nanotechnol.* **2017**, *12*, 1134–1139. [CrossRef]
48. Beard, M.C.; Knutsen, K.P.; Yu, P.R.; Luther, J.M.; Song, Q.; Metzger, W.K.; Ellingson, R.J.; Nozik, A.J. Multiple exciton generation in colloidal silicon nanocrystals. *Nano Lett.* **2007**, *7*, 2506–2512. [CrossRef] [PubMed]
49. Ouyang, T.H.; Wang, X.M.; Liu, S.J.; Chen, H.J.; Deng, S.Z. A Complete Two-Dimensional Avalanche Photodiode Based on $MoTe_2$-WS_2-$MoTe_2$ Heterojunctions with Ultralow Dark Current. *Front. Mater.* **2021**, *8*, 736180. [CrossRef]
50. Yang, Y.J.; Jeon, J.; Park, J.H.; Jeong, M.S.; Lee, B.H.; Hwang, E.; Lee, S. Plasmonic Transition Metal Carbide Electrodes for High-Performance InSe Photodetectors. *ACS Nano* **2019**, *13*, 8804–8810. [CrossRef]
51. Lei, S.D.; Wen, F.F.; Ge, L.H.; Najmaei, S.; George, A.; Gong, Y.J.; Gao, W.L.; Jin, Z.H.; Li, B.; Lou, J.; et al. An Atomically Layered InSe Avalanche Photodetector. *Nano Lett.* **2015**, *15*, 3048–3055. [CrossRef]
52. Li, X.; Chen, J.; Yu, F.L.; Chen, X.S.; Lu, W.; Li, G.H. Achieving a Noise Limit with a Few-layer WSe_2 Avalanche Photodetector at Room Temperature. *Nano Lett.* **2024**, *24*, 13255–13262. [CrossRef] [PubMed]
53. Jia, J.Y.; Jeon, J.; Park, J.H.; Lee, B.H.; Hwang, E.; Lee, S. Avalanche Carrier Multiplication in Multilayer Black Phosphorus and Avalanche Photodetector. *Small* **2019**, *15*, 1805352. [CrossRef]
54. Zhang, Z.Y.; Cheng, B.; Lim, J.; Gao, A.Y.; Lyu, L.Y.; Cao, T.J.; Wang, S.; Li, Z.A.; Wu, Q.Y.; Ang, L.K.; et al. Approaching the Intrinsic Threshold Breakdown Voltage and Ultrahigh Gain in a Graphite/InSe Schottky Photodetector. *Adv. Mater.* **2022**, *34*, e2206196. [CrossRef] [PubMed]
55. Wang, H.L.; Xia, H.; Liu, Y.Q.; Chen, Y.; Xie, R.Z.; Wang, Z.; Wang, P.; Miao, J.S.; Wang, F.; Li, T.X.; et al. Room-temperature low-threshold avalanche effect in stepwise van-der-Waals homojunction photodiodes. *Nat. Commun.* **2024**, *15*, 3639. [CrossRef]
56. Chen, Y.; Wei, W.R.; Wang, H.L.; Bai, Y.Z.; Zhang, T.; Zhang, K.; Duan, S.K.; Yu, Y.Y.; Zhao, T.E.; Xie, R.Z.; et al. Room-Temperature WSe_2 Impact Ionization Field-Effect Transistor Based on a Stepwise Homojunction. *Small* **2025**, 2412466. [CrossRef] [PubMed]
57. Son, B.; Wang, Y.D.; Luo, M.L.; Lu, K.Z.; Kim, Y.; Joo, H.J.; Yi, Y.; Wang, C.W.; Wang, Q.J.; Chae, S.H.; et al. Efficient Avalanche Photodiodes with a WSe_2/MoS_2 Heterostructure via Two-Photon Absorption. *Nano Lett.* **2022**, *22*, 9516–9522. [CrossRef]
58. Wu, G.J.; Wang, X.D.; Chen, Y.; Wu, S.Q.; Wu, B.M.; Jiang, Y.Y.; Shen, H.; Lin, T.; Liu, Q.; Wang, X.R.; et al. $MoTe_2$ p-n Homojunctions Defined by Ferroelectric Polarization. *Adv. Mater.* **2020**, *32*, 1907937. [CrossRef]
59. Wei, X.; Yan, F.G.; Lv, Q.S.; Zhu, W.K.; Hu, C.; Patanè, A.; Wang, K.Y. Enhanced Photoresponse in $MoTe_2$ Photodetectors with Asymmetric Graphene Contacts. *Adv. Opt. Mater.* **2019**, *7*, 1900190. [CrossRef]

60. Gao, A.Y.; Lai, J.W.; Wang, Y.J.; Zhu, Z.; Zeng, J.W.; Yu, G.L.; Wang, N.Z.; Chen, W.C.; Cao, T.J.; Hu, W.D.; et al. Observation of ballistic avalanche phenomena in nanoscale vertical InSe/BP heterostructures. *Nat. Nanotechnol.* **2019**, *14*, 217–222. [CrossRef] [PubMed]
61. Lin, J.; Chen, X.Z.; Duan, X.P.; Yu, Z.M.; Niu, W.C.; Zhang, M.L.; Liu, C.; Li, G.L.; Liu, Y.; Liu, X.Q.; et al. Ultra-Steep-Slope High-Gain MoS_2 Transistors with Atomic Threshold-Switching Gate. *Adv. Sci.* **2022**, *9*, 2104439. [CrossRef]
62. Kim, S.G.; Kim, S.H.; Kim, G.S.; Jeon, H.; Kim, T.; Yu, H.Y. Steep-Slope Gate-Connected Atomic Threshold Switching Field-Effect Transistor with MoS_2 Channel and Its Application to Infrared Detectable Phototransistors. *Adv. Sci.* **2021**, *8*, 2100208. [CrossRef]
63. Hua, Q.L.; Gao, G.Y.; Jiang, C.S.; Yu, J.R.; Sun, J.L.; Zhang, T.P.; Gao, B.; Cheng, W.J.; Liang, R.R.; Qian, H.; et al. Atomic threshold-switching enabled MoS_2 transistors towards ultralow-power electronics. *Nat. Commun.* **2020**, *11*, 6207. [CrossRef]
64. Wang, X.F.; Tian, H.; Liu, Y.M.; Shen, S.H.; Yan, Z.Y.; Deng, N.Q.; Yang, Y.; Ren, T.L. Two-Mode MoS_2 Filament Transistor with Extremely Low Subthreshold Swing and Record High On/Off Ratio. *ACS Nano* **2019**, *13*, 2205–2212. [CrossRef]
65. Liu, Y.; Guo, J.; Song, W.J.; Wang, P.Q.; Gambin, V.; Huang, Y.; Duan, X.F. Ultra-Steep Slope Impact Ionization Transistors Based on Graphene/InAs Heterostructures. *Small Struct.* **2021**, *2*, 2000039. [CrossRef]
66. Gao, A.Y.; Zhang, Z.Y.; Li, L.F.; Zheng, B.J.; Wang, C.Y.; Wang, Y.J.; Cao, T.J.; Wang, Y.; Liang, S.J.; Miao, F.; et al. Robust Impact-Ionization Field-Effect Transistor Based on Nanoscale Vertical Graphene/Black Phosphorus/Indium Selenide Heterostructures. *ACS Nano* **2020**, *14*, 434–441. [CrossRef]
67. Choi, H.; Li, J.; Kang, T.; Kang, C.; Son, H.; Jeon, J.; Hwang, E.; Lee, S. A steep switching WSe_2 impact ionization field-effect transistor. *Nat. Commun.* **2022**, *13*, 6076. [CrossRef] [PubMed]
68. Martyniuk, P.; Wang, P.; Rogalski, A.; Gu, Y.; Jiang, R.; Wang, F.; Hu, W. Infrared avalanche photodiodes from bulk to 2D materials. *Light-Sci. Appl.* **2023**, *12*, 2095–5545. [CrossRef] [PubMed]
69. Wang, B.H.; Mu, J.F. High-speed Si-Ge avalanche photodiodes. *PhotoniX* **2022**, *3*, 8. [CrossRef]
70. Liu, J.X.; Peng, Z.H.; Tan, C.; Yang, L.; Xu, R.D.; Wang, Z.G. Emerging single-photon detection technique for high-performance photodetector. *Front. Phys.* **2024**, *19*, 62502. [CrossRef]
71. Lozovoy, K.A.; Douhan, R.M.H.; Dirko, V.V.; Deeb, H.; Khomyakova, K.I.; Kukenov, O.I.; Sokolov, A.S.; Akimenko, N.Y.; Kokhanenko, A.P. Silicon-Based Avalanche Photodiodes: Advancements and Applications in Medical Imaging. *Nanomaterials* **2023**, *13*, 3078. [CrossRef]
72. Abbasi, R.; Hu, X.Y.; Zhang, A.; Dummer, I.; Wachsmann-Hogiu, S. Optical Image Sensors for Smart Analytical Chemiluminescence Biosensors. *Bioengineering* **2024**, *11*, 912. [CrossRef]
73. Yuan, B.W.; Chen, Z.B.; Chen, Y.X.; Tang, C.J.; Chen, W.A.; Cheng, Z.G.; Zhao, C.S.; Hou, Z.Z.; Zhang, Q.; Gan, W.Z.; et al. High drain field impact ionization transistors as ideal switches. *Nat. Commun.* **2024**, *15*, 9038. [CrossRef]
74. Choi, H.; Baek, S.; Jung, H.; Kang, T.; Lee, S.; Jeon, J.; Jang, B.C.; Lee, S. Spiking Neural Network Integrated with Impact Ionization Field-Effect Transistor Neuron and a Ferroelectric Field-Effect Transistor Synapse. *Adv. Mater.* **2024**, 2406970. [CrossRef] [PubMed]
75. Li, L.; Li, S.S.; Wang, W.H.; Zhang, J.L.; Sun, Y.M.; Deng, Q.R.; Zheng, T.; Lu, J.T.; Gao, W.; Yang, M.M.; et al. Adaptative machine vision with microsecond-level accurate perception beyond human retina. *Nat. Commun.* **2024**, *15*, 6261. [CrossRef] [PubMed]